(Received 22 June 2023, Accepted 4 November 2023, Scheduled 14 November 2023)

Coaxial Pin-Fed Multiband Fractal Square Antenna for Satellite Applications

Varnikha Nanthagopal[1,*] and Jothilakshmi Paramasivam[1]

[1] Department of Electronics and communication Engineering, Sri Venkateswara college of Engineering, Sriperambudur, India

ABSTRACT: A coaxially pin-fed multiband fractal square antenna is proposed in this paper. The designed antenna resonates in five bands: 5 GHz, 10 GHz, 13.2 GHz, 16 GHz, and 20.5 GHz. The multibands are achieved by using a fractal square antenna. The fractal square is formed from an initial square patch and then optimized with increasing fractal iterations to resonate at these bands. The fractal property of the design also helps in the miniaturisation of the antenna. The proposed antenna has gain ranging from 4.9 dB to 9.7 dB and radiation efficiencies from 70% to 98%. The proposed antenna is simulated using the CST microwave studio. The antenna is then fabricated, and its performance parameters are measured. After finding a match between simulated and measured results, the same antenna and its array are tested in a MATLAB simulation environment for direction of arrival (DOA) and adaptive beamforming (AB) at all five bands. Using different DOA and AB algorithms, the performance of the antenna array is evaluated. The ability to accurately estimate the DOA of all signals delivered to the adaptive array antenna allows it to maximise its performance in terms of recovering the required transmitted signal and suppressing any interference signal. Then, the beam of the antenna is modified using the DOA algorithm to generate a beam in the desired direction and nulls in the unwanted direction for proposed satellite communications.

1. INTRODUCTION

Broadcast television transmissions, internet delivery, data communication, voice telephony, and aviation systems all make use of satellite communications technologies operating in the C band. When national administrations permit broadband wireless access systems like Wi-Fi and Wi-Max to share the same spectrum bands currently used by satellite services, the satellite systems operating in the C band experience severe interference, sometimes to the point of system failure [1]. The use of the Standard C and Extended C bands for terrestrial wireless networks poses a serious danger to satellite services. Hence, the SATCOM industry has moved to higher frequency bands to avoid this congestion. ITU has defined new bands such as X, Ku, K, and Ka bands for SATCOM [2]. Here, high-speed communication can be achieved by using small antennas with a larger bandwidth of operation. Due to the higher wavelength in the C band, the signals are less affected by rain and other obstacles, but the attenuation due to rain is greater in the Ku and Ka bands due to their smaller wavelengths [3]. Hence, we can use C-band antennas in places with frequent rainfall density areas, and in other locations, we can go for K or Ku-band antennas for SATCOM.

The present work proposes a fractal antenna resonating at multiple bands that allows simultaneous reception of RF signals from different satellites transmitting at multiple frequencies. In such cases, higher bands (Ku and K bands) can be used for high-resolution images and video transmissions with high bandwidth requirements, and lower bands (C and X bands) can be used for low-bandwidth data transmissions like voice and text messages. In today's world, many such applications necessitate the utilisation of multiband antennas as opposed to single band antennas in order to mitigate costs and complexities. Hence, in this paper, a multiband antenna is proposed which can operate in C, X, Ku, and K bands.

The main limitation of a multiband antenna is its inability to sustain gain and radiation patterns over all the resonating bands. The addition of slots to the antenna's radiating surface can cause the antenna to resonate across various frequency bands. It is well known that slots generate multibands and operate as numerous radiating elements, resulting in multiresonant behaviour. By modifying the current flow, this can shift the antenna's working frequency, thereby shifting the frequency to a higher or lower band. A planar multiband antenna with a hexagonal patch is constructed [4]. On the hexagonal patch, two pairs of modified L-shaped resonator slots are etched to provide multibands. To increase the impedance bandwidth of the patch antenna, several types of defects are introduced at the ground. Defected Ground Structure (DGS) is a technique used to increase the impedance bandwidth of an antenna and explore additional resonance frequencies. In [5], a four-band patch antenna with DGS is proposed and tested. Another fundamental method for creating multiband antennas is multi-layered structuring [23], which includes stacking a number of microstrip patches that operate over a variety of frequencies vertically onto a ground plane to increase the antenna's height. [24] presents a miniaturised multiband two-element coaxial continuous transverse stub antenna for satellite C-band applications. The continuous transverse stub (CTS) technology incorporates the use of coaxial lines to produce effective microwave antenna structures that radiate an omnidirectional pattern with high efficiency and low return loss. For multiband

* Corresponding authors: Varnikha Nanthagopal (varnikavidesh@gmail.com).

applications, [6] presents a substrate-integrated suspended-line (SISL) triple-band multi-mode antenna with a stacked patch and two L-strips. To create two resonant frequencies, two L-strips coupled to the stacked patch by vias are inserted. The stacked patch and via, which connect the feed line and driven patch, respectively, produce resonant frequencies in the higher frequency region. Metamaterials are artificial materials that are designed to have properties that are not found in naturally occurring materials. Metamaterials also have the advantage of being able to operate in multiple frequency bands. This is due to their ability to tailor both permittivity and permeability independently, which allows them to interact with electromagnetic waves in a variety of ways, resulting in multiple bands. [7, 8] exhibit metamaterial-based multiband antennas comprising complementary split-ring resonators. A multiband antenna that is loaded with parasitic components is presented in [9]. The radiator has a loop of nested hexagons with a top opening. A microstrip line with two parasitic components at the top feeds the three hexagonal open loops, which have a small hexagonal radiator in the centre that provides the multiband. [10] presents the design of a CPW-fed, metamaterial-inspired, octagon-shaped antenna on a frequency-selective surface (FSS) for multiband operations. This antenna is ideal for 5G mobile communications and satellite applications.

Miniaturised high-gain multiband antennas [11–13] can also be efficiently designed using fractals. Self-similarity and replication at different sizes characterise the fractal antenna, which efficiently fills the available area. Due to the property of self-similarity, fractal antennas exhibit multiband behaviour. Since small regions of fractal geometry are copies of the entire structure on a smaller scale, identical electromagnetic behaviour can be achieved at various frequencies. The space-filling feature of a fractal structure allows for the creation of extremely long lengths or broad surfaces in a compact area [22]. Fractals can be used in antenna design to meet multiband, wideband, and size reduction goals. Antennas have been designed using a wide variety of fractal patterns, including Hilbert curves, Sierpinski gaskets, and Koch snowflakes. The multiband antennas designed above do not have constant gain and stable radiation pattern over all the resonating bands. Hence, there is a need to design a multiband antenna with constant gain, stable radiation pattern, and high efficiency over all resonating bands covering 2–3 bands for satellite communication.

Here, we have used the fractal concept to design our multiband antenna. Different iterations of the fractal are realized to achieve the required bands for satellite communications. Later, the same antenna and its array are tested in a MATLAB simulation environment. The performance of the antenna and its array are evaluated with different Direction of Arrival (DOA) [20] and Adaptive Beamforming (AB) algorithms [21] to find the best for satellite communication. After finding the best-case scenario for both DOA and AB for the first resonating band, all four other bands of the proposed antenna are tested with the best DOA and AB algorithms. The article is structured as follows. The fractal antenna is designed with multiple iterations in Section 2. All the simulated and measured results are discussed in Section 3. The performances of the proposed antenna are compared with other similar designs from literature in the same section. Then, the proposed antenna and its array are evaluated for different DOA and AB algorithms in MATLAB in Section 4. Finally, the article is concluded in Section 5.

2. PROPOSED FRACTAL ANTENNA DESIGN

Figure 1 shows the structure of the proposed multiband microstrip patch antenna. The antenna is printed on a Rogers RT 5880 substrate with Epsilon 2.2 and substrate thickness 0.787 mm. The size of the ground plane is 32 mm by 32 mm. By using the parameters frequency, ε_r, and h, and with the help of the following equations, dimension of the microstrip patch antenna (MPA) is evaluated.

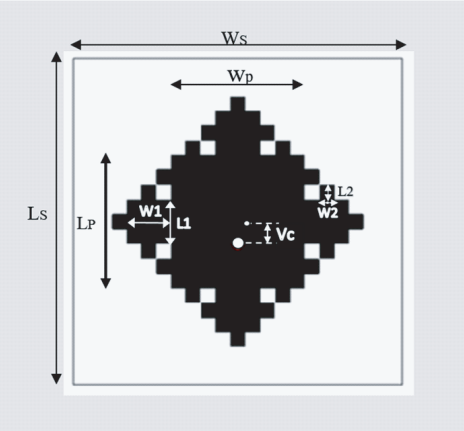

FIGURE 1. Design of the proposed multiband fractal antenna. ($Ws = Ls = 32$, $Wp = Lp = 13$, $W1 = L1 = 4.3$, $W2 = L2 = 1.3$, all units in mm).

The width (W) of the antenna is calculated by the following formula.

$$W = \frac{1}{2f_r\sqrt{\mu_0 \in_0}}\sqrt{\frac{2}{\in_r +1}} \tag{1}$$

Substituting ε_r, h, and calculated W value in the following equation, the effective dielectric constant (ε_{reff}) and the extensive length (ΔL) are calculated.

$$\in_{reff} = \frac{\in_r +1}{2} + \frac{\in_r -1}{2}\left[1 + 12\frac{h}{W}\right]^{-\frac{1}{2}} \tag{2}$$

$$\Delta L = 0.412h\frac{(\in_{reff} +0.3)\left(\frac{W}{h} + 0.264\right)}{(\in_{reff} -0.258)\left(\frac{W}{h} + 0.8\right)} \tag{3}$$

Now, the actual length (L) of the MPA is found out by the following equation.

$$L = \frac{1}{2f_r\sqrt{\in_{reff}}\sqrt{\mu_0 \in_0}} - 2\Delta L \tag{4}$$

As the width of the patch is much smaller than the operating wavelength, the input resistance at the edge ($R_{in}(y = 0)$) of the patch can be evaluated from:

$$G_1 = \frac{1}{90}\left(\frac{W}{\lambda_0}\right)^2 \quad for\ W \ll \lambda \tag{5}$$

$$R_{in}(y=0) = \frac{1}{2G_1} \tag{6}$$

The radiator of the proposed antenna is a fractal square-shaped structure, which is fed by a simple coaxial pin feed. The distribution of impedance is minimum at the centre and maximum on both edges of the patch. So there is a point inside the surface of the radiating patch where the impedance is 50 Ω. The simplest method for impedance matching is to locate the position of the 50 Ω point and connect the feed probe at this point. The microstrip line must have the appropriate width to match the patch with the feed line. The width of the microstrip feed line (W_0) and distance y_0 can be calculated by using following equations.

$$Z_0 = \frac{60}{\sqrt{\epsilon_{reff}}} \ln\left[\frac{8h}{W_0} + \frac{W_0}{4h}\right] \tag{7}$$

$$R_{in}(y=y_0) = R_{in}(y=0)\cos^2\left(\frac{\pi}{L}\right)y_0 \tag{8}$$

where L is the length of the patch; the required impedance $R_{in}(y = y_0)$ is 50 Ω; and the edge impedance $R_{in}(y = 0)$ is 209.268 Ω. y_0 is found to be 4.4 from the above equation. The position of the feed from center (Vc) calculated from it was found to be 2.1 mm to match the 50 Ω impedance.

The antenna is designed in three steps using an initiator and generator structure. The starting shape is known as an initiator. As seen in Figure 2, a generator is an ordered collection of scaled replicas of the initiator. Replace each copy of the initiator with a scaled copy of the generator at each stage, i.e., replace each line segment with the scaled copy of the generator as illustrated in Figure 3. Step 1 involves replacing a single line segment in the initiator with the generator. In the second step, each of the four line segments from the first step has to be replaced with a scaled copy of the generator. There are four line segments in step 1. Hence, step 1 requires a total of four copies of the generator. Step 2 includes 20 line segments. As a result, step 2 necessitates the use of twenty copies of the scaled generator.

FIGURE 2. Structure of initiator and generator for fractal design.

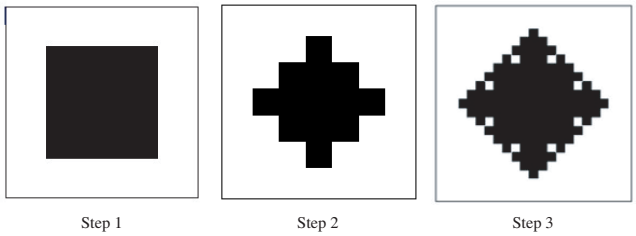

FIGURE 3. Fractal antenna design stages.

The square side length of the first generation is 13 mm. A square of side length 4.33 mm is placed on each side of the first generation square to get the second generation. The square of side length 1.4 is the third generation. All the sides of the square are reduced by a factor of 1/3 to maintain self-similarity. The scaling that occurs between generations is determined by a fixed value called 'f' that lies within the range 0 to 1, and it is set up in such a way that the $n + 1$ generation has a square side-length that is f times smaller than the nth generation. This reduction in size between generations helps to maintain self-similarity. $n + 1$ generation squares are attached only to the exposed edges of the nth generation elements.

3. RESULTS AND DISCUSSION

Antenna performance can be analysed by its reflection and radiation characteristics. The scattering parameter, or S-parameter, determines how the antenna radiates or receives power. The return loss plots for Step 1, Step 2, and Step 3 are included in Figure 4. Voltage standing wave ratio (VSWR) is less than 2 for all the 5 resonating bands of step 3, which can be seen from Figure 5. It is illustrated from the VSWR graph that the proposed antenna shows the required multiband characteristics. The antenna resonates over 5 frequency bands with operating frequencies of 5 GHz, 10 GHz, 13.2 GHz, 16.2 GHz, and 20.5 GHz. The first frequency band is 57 MHz; the second frequency band is 49 MHz; the third frequency band is 386 MHz; the fourth frequency band is 558 MHz; and the last frequency band is 343 MHz. Here, Step 1, Step 2, and Step 3 are designated as Design 1, Design 2, and Design 3, respectively. Design 3 is the final modification for the proposed fractal antenna.

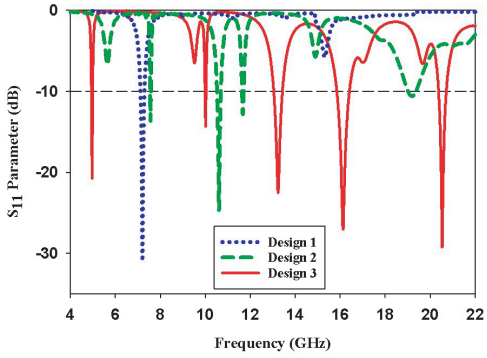

FIGURE 4. S_{11} plots of Design 1, Design 2, and Design 3 of the proposed square fractal antenna.

Figure 6 shows the surface current distribution for the proposed fractal antenna at all five frequencies. The different colours represent the different magnitudes of current. Red is the maximum value, and blue represents the least value in magnitude of the surface current. At the lower frequency, the current is distributed almost all over the patch. By introducing perturbations at the boundary, we can alter the distribution of surface current, which tends to cause the antenna to resonate at different frequencies.

The gain of the antenna is shown in Figure 7. The gain and radiation efficiency of the antenna are stabilized at multiple resonating frequencies by realizing repetitive fractal design

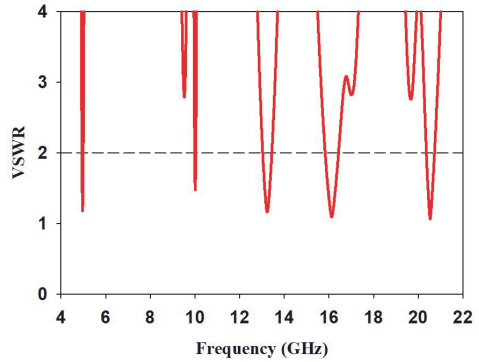

FIGURE 5. VSWR of the proposed fractal square antenna.

with self-similar properties. The maximum gains obtained are 6.6 dB, 4.9 dB, 5.5 dB, 7.8 dB, and 9.7 dB at 5 GHz, 10 GHz, 13.2 GHz, 16.2 GHz, and 20.5 GHz, respectively. The radiation efficiency of the radiating element is mostly determined by the impedance match between the port and the element. The efficiency of the proposed antenna at 5 GHz, 10 GHz, 13.2 GHz, 16.2 GHz, and 20.5 GHz is 77%, 70%, 98%, 94%, and 90%, respectively, as shown in Figure 8.

The prototype of the antenna is fabricated, and its performance parameters are measured as shown in Figure 9. The reflection characteristics of the fabricated prototype are measured with a vector network analyzer. The simulated and measured S-parameters are shown in Figure 10. The results reveal that reasonable agreement between measurements and simulations has been achieved. The proposed fabricated antenna also resonates in five bands, as discussed. A minor mismatch is found between the simulated and measured S_{11} due to a possible fabrication error at the feed connection point.

The fabricated antenna was then placed in an anechoic chamber for radiation pattern measurement. In this setup, a horn antenna is placed as the transmitter antenna, and the proposed antenna is placed as an antenna under test (AUT). The received power at the AUT is noted against the angle for all five resonating frequencies. Then, the gain of the proposed antenna is calculated and plotted using Frii's equation. Figure 11 shows the radiation pattern match between simulated patterns and measured patterns at all five frequencies. The radiation patterns are plotted for both the E and H planes. From the figure, it can be seen that a matching pattern is found between the simulated and measured patterns. These matchings found both in reflection and radiation characteristics prove the authenticity of the proposed design and its concept.

Table 1 comprises a comparison of performance parameters among the proposed antenna and other similar designs available in the literature. Among all the designs, [19] and the proposed design have achieved the most resonant frequencies. However, the range of gain in [19] is from -1.8 dB to 6.2 dB, which is less than the proposed design with a gain range of 6.6 dB to 9.7 dB. Compared to all other designs, our proposed antenna has the maximum gain and radiation efficiencies with five resonating bands. As the designs compared here resonate at different frequencies, it is unfair to compare their sizes in terms of mm. So, the sizes of all the designs are compared here in terms of their lowest operating wavelength. The proposed design has the size of $0.53\lambda * 0.53\lambda$ compared to other designs. From these comparisons, it can be concluded that the fractal design proposed here may not be the best among all the similar designs available, but most importantly, it has balanced performance characteristics with a stable gain and radiation pattern at all five resonating bands. This makes the proposed design a perfect choice for satellite applications. Finally, the performance of the proposed antenna is evaluated in MATLAB simulation environments. The reflection and radiation characteristics of the antenna are exported to MATLAB, and a replica of the design and its array is developed in MATLAB. Then, different Direction of Arrival (DOA) and Adaptive Beamforming (AB) algorithms are tested to determine which is best suited for the proposed antenna. Finally, the desired signal is received with the best-found DOA and AB algorithms for all five resonating frequencies. All these procedures and steps in MATLAB are discussed in detail in the coming section.

4. DOA AND AB OF PROPOSED ANTENNA IN MATLAB

With an increasing number of wireless users, smart antennas are being employed to replace traditional antenna systems in order to enhance system efficiency and reduce co-channel interference. An antenna array with a beam-forming network [18], microwave circuitry, and signal processing units comprises a smart antenna. Reflector antennas are commonly used for satellite earth stations because of their high gain, large bandwidth, and inexpensive cost. Yet they are large and can only monitor satellites through mechanical movement. To communicate with numerous satellites, several reflector antennas are also required. However, several satellites can be tracked with a single smart antenna. Smart antennas are used to estimate the signal's direction of arrival (DOA). DOA estimation and beamforming are the two most important aspects of smart antennas. The ability to accurately estimate the DOA of all signals delivered to the adaptive array antenna allows it to maximise its performance in terms of recovering the required transmitted signal and suppressing any interference signal. The beam of the smart antenna can be modified using the DOA algorithm [17] to generate a beam in the desired direction and nulls in the undesired direction.

The DOA method is applied to signal samples taken from each element of the array in order to calculate an estimate of the direction from which incoming signals are coming. The signals that have been detected are then classified as either signals of interest or signals not of interest. Then beamforming algorithms are used to compute the necessary weights, obtain the desired pattern, and point the antenna in the direction of interest of signals.

Smart antenna systems consist of antenna arrays. For designing an array, we import the pattern from CST to MATLAB, design a custom antenna, and create an array in MATLAB to test our antenna. To design an array in MATLAB, we first need to specify the number of elements in the array and their spacing. We can use various array geometries, such as linear, circular, or planar one, depending on the application requirements. Next, we use the custom antenna designed to specify the element pat-

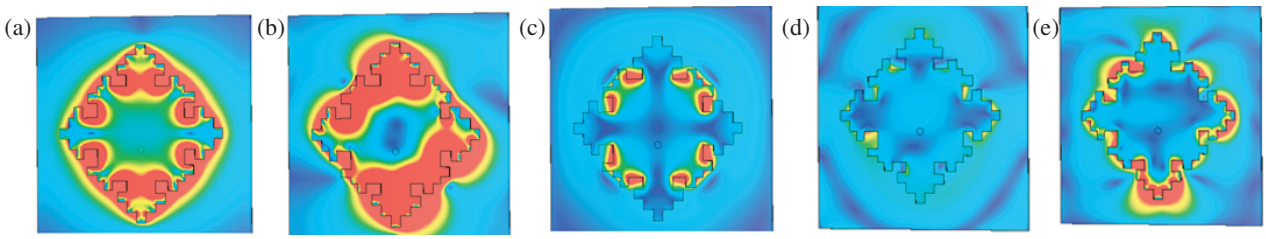

FIGURE 6. Surface current distribution at (a) 5 GHz, (b) 10 GHz, (c) 13.2 GHz, (d) 16.2 GHz, and (e) 20.5 GHz.

TABLE 1. Comparison table among the proposed design with other designs available in the literature.

Reference	Dimension	Resonating Frequency (GHz), Bandwidth (MHz)	Gain (dB)	Efficiency (%)
[14] 2014	$0.52\lambda * 0.60\lambda$	8.95, 450 11.06, 1010 11.85, 450	(3.99–4.45)	95
[15] 2017	$0.85\lambda * 0.85\lambda$	12.07, 130 14.44, 120	(4.8–7.4)	78
[16] 2017	$0.75\lambda * 0.51\lambda$	4.53, 70 5.01, 20 5.47, 20	(5–5.9)	86
[17] 2018	$0.54\lambda * 0.54\lambda$	3.24, 400 5.17, 200 5.85, 100	(2.25–4.11)	80
[18] 2020	$0.80\lambda * 0.80\lambda$	12.25, 1510 14.16, 670 17.5, 660	(2–6)	70
[19] 2021	$0.68\lambda * 0.60\lambda$	5.16, 350 6.6, 200 7.2, 380 8.3, 600 9.96, 1100	(−1.8–6.2)	NA
[25] 2023	$0.44\lambda * 0.24\lambda$	0.77, 150 1.37, 550 2.12, 750	2.4–4	81
[26] 2023	$0.82\lambda * 0.79\lambda$	5.1, 850 6.6, 325 8.2, 469	2.78–5.91	69
[27] 2023	$0.42\lambda * 0.42\lambda$	1.56, 40 2.49, 90 3.5, 100 5.24, 90	3.49–6.49	95
Proposed antenna	**$0.53\lambda * 0.53\lambda$**	5, 57 10, 49 13.2, 386 16.2, 558 20.5, 343	6.6 4.9 5.5 7.8 **9.7**	77 70 98 **98** 94 90

tern for each element in the array. Finally, we combine the individual element patterns and obtain the overall radiation pattern

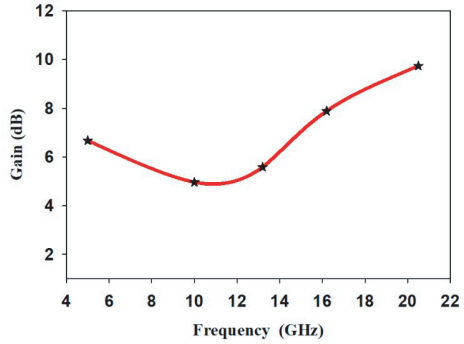

FIGURE 7. Total Gain of the antenna at (a) 5 GHz, (b) 10 GHz, (c) 13.2 GHz, (d) 16.2 GHz, and (e) 20.5 GHz.

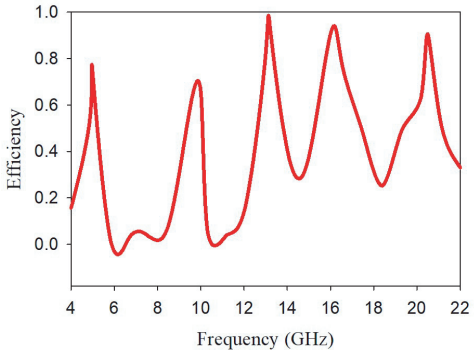

FIGURE 8. Radiation Efficiency of the antenna.

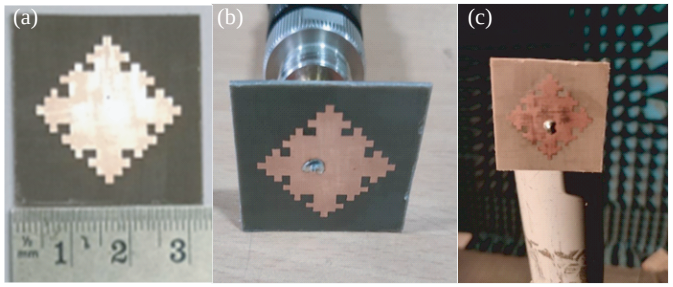

FIGURE 9. (a) Fabricated antenna with scale, (b) Antenna connected with VNA, (c) Antenna in anechoic chamber.

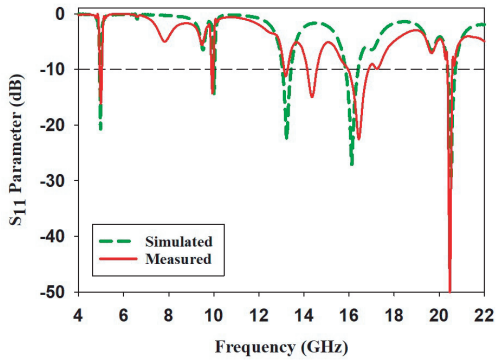

FIGURE 10. Simulated and measured S_{11} vs. frequency for the proposed antenna.

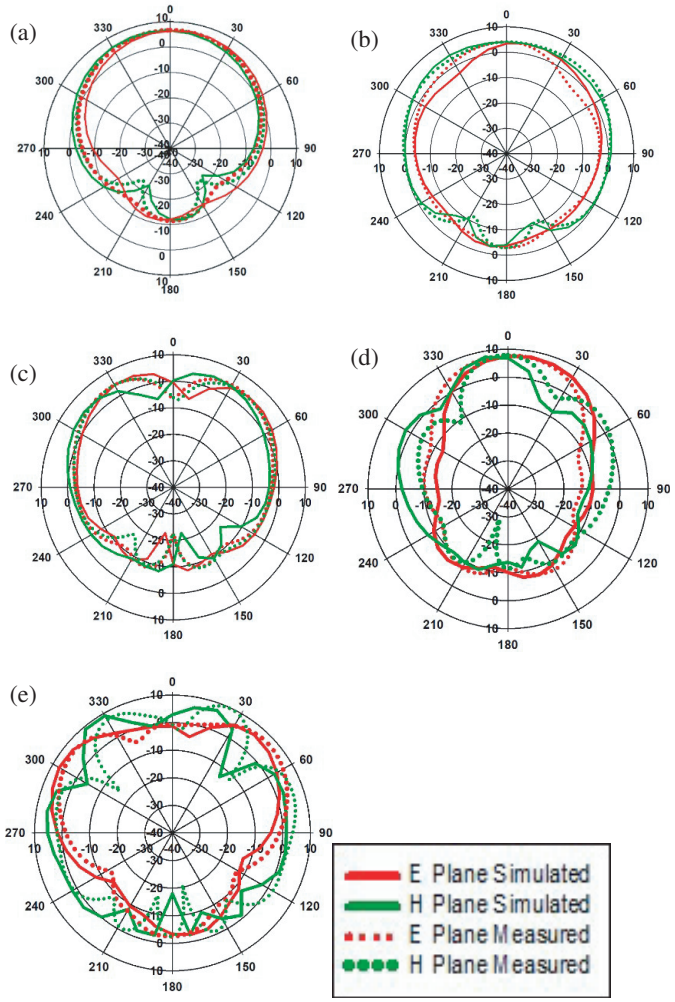

FIGURE 11. Simulated and measured E-plane and H-plane radiation patterns at (a) 5 GHz, (b) 10 GHz, (c) 13.2 GHz, (d) 16.2 GHz, and (e) 20.5 GHz.

of the array. Once the array is designed, we can use MATLAB to simulate its performance in different scenarios, such as varying the direction of the incident wave. This can help us optimise the design of the array and ensure that it meets the desired performance requirements. Overall, designing a custom antenna and array in MATLAB allows us to simulate their performance and optimise their design before actually building them. This can save time and resources and ensure that the final product meets the desired performance specifications. For this, we need to first import the radiation pattern of our antenna for all the frequencies from CST to MATLAB. An M-by-3 matrix is used in CST to represent the simulated radiation pattern. The first column of this matrix indicates the angle ϕ; the second column represents the angle θ; and the third column represents the radiation pattern in dB. It is considered that the antenna's main beam is oriented along the Z axis. The range for ϕ is 0 to 360 degrees, and the range for θ is 0 to 180 degrees. However, azimuth and elevation angles are used to express the radiation pattern in MATLAB. It is presumed that the primary beam of the antenna is aimed in the direction of 0 degrees of azimuth and 0 degrees of elevation, which is the x axis. The azimuth

value ranges from −180 to 180 degrees, and the elevation value ranges from −90 to 90 degrees. Thus, to import the values of ϕ between 0 and 360 and convert them into azimuth values between −180 and 180 degrees, as well as to import the values of θ between 0 and 180 degrees and convert them into elevation values between −90 and +90 degrees, the CST pattern import MATLAB function is used. The steps involving all this are discussed in detail in the flowchart in Figure 12.

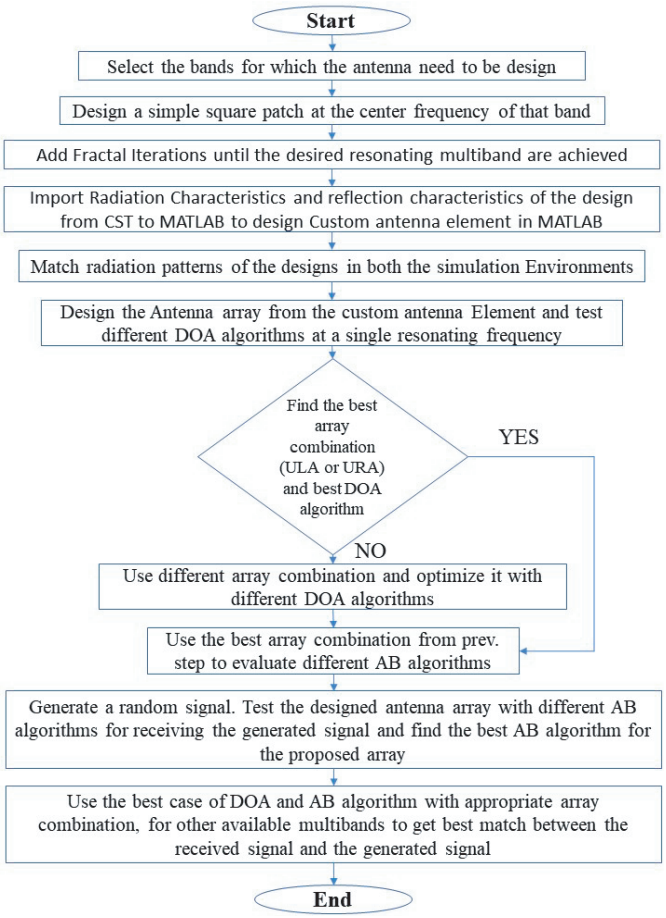

FIGURE 12. Flow chart describing the whole process, starting from the multiband fractal antenna design, fabrication, and testing in MATLAB for DOA and AB.

At first, we import the frequency vector. Then we include the gain and pattern of the antenna in all the frequencies. After importing the radiation pattern data into MATLAB using the command CST pattern import MATLAB, we create a custom antenna. The custom antenna can be created using the specified radiation pattern, frequency range, and gain of the antenna designed in CST.

After designing a custom antenna from a corresponding antenna in CST, we can confirm that they are the same antenna by comparing their radiation patterns. The radiation pattern of an antenna is the spatial distribution of the electromagnetic fields radiated by the antenna. It provides information about the antenna's directivity, gain, and polarization. Once the custom antenna is designed in MATLAB, we can use it to design an array. An array is a collection of multiple antennas that work together to achieve a desired radiation pattern. 3D radiation patterns of the proposed antenna are compared in Figure 13 in both the simulation environments of CST and MATLAB. From the figure, a good match is found, which proves the accuracy of the replicated custom antenna design in MATLAB.

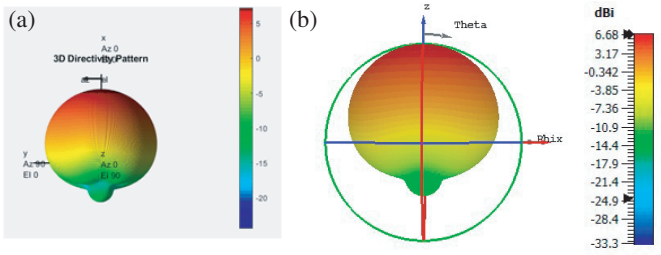

FIGURE 13. 3D directivity pattern in (a) MATLAB and (b) CST for the designed antenna.

For further analysis of DOA and AB, an array needs to be designed from the custom antenna in MATLAB. Hence, our smart antenna system consists of a uniform linear array of the proposed antenna with 10 elements that are spaced linearly at a distance of lambda/2. The array geometry is shown in Figure 14(a). The 3D directivity pattern of the array is shown in Figure 14(b), with a maximum directivity of 15 dB.

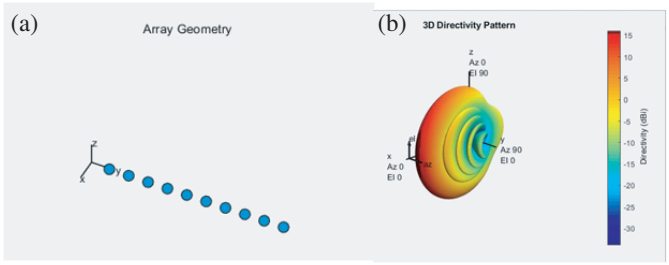

FIGURE 14. (a) Linear antenna array geometry and (b) 3D directivity pattern of array.

After the construction of the linear array, several DOA algorithms are then applied to the array. Minimum variance distortion less response (MVDR), multiple signal classification (MUSIC), and beam scan algorithms are all useful techniques for estimating the direction of arrival of signals in various applications. The MVDR algorithm is a signal processing technique that is used to estimate the DOA of signals in the presence of noise and interference. The algorithm works by computing a set of weights for a linear array of sensors such that the response in the direction of the desired signal is maximized while the response in the directions of the noise and interference sources is minimized. The resulting MVDR beamformer output is a signal that has a minimum variance and is therefore free from distortion. Similarly, the beam scan algorithm is another technique that is used for DOA estimation. It works by steering a beam of sensors in different directions and measuring the received signals. The signals are then processed to estimate the DOAs of the sources. The performance of the smart antenna relies on an accurate estimation of DOA. Conventionally, a beam scanning algorithm was used to estimate DOA. Assume that two narrowband signals impinge on the array. The first signal arrives from 30° in azimuth, and the second signal arrives from 35° in azimuth, but when the two signals are closely spaced, the beam

scanning algorithm wrongly detects the incoming signal. The power responses of all three algorithms are compared in Figure 15. The beam scanner estimates the DOA at 32 degrees. To resolve this problem, we use the MVDR algorithm and MUSIC algorithm. The MVDR algorithm correctly estimates the DOAs that are unresolvable by beam scanning. The MUSIC algorithm gives maximum power in the directions of interest and minimum power in directions not of interest. In the beam scan algorithm, we get side lobes. In MVDR, we do not get the side lobes. The MUSIC algorithm gives an even more accurate spectrum.

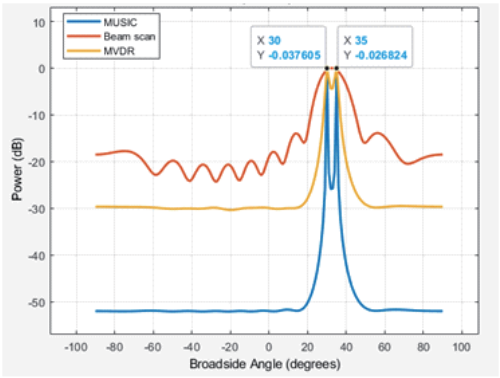

FIGURE 15. DOA spectrum of beam scan, MVDR and MUSIC algorithms.

In the next step, we examine the sources that are even closer together to compare the performances of the MVDR and MUSIC estimators for the proposed array. Compute the spatial spectrum of two sources located at 10° in azimuth and separated by 2° in elevation (40 and 42 degrees) using MVDR and MUSIC. In this particular instance, only MUSIC provides estimations that are accurate regarding the directions of arrival for the two sources, which are 40 and 42 degrees, respectively, as shown in Figure 16. The MUSIC spectrum, which has higher spatial resolution than the MVDR spectrum, is able to correctly identify the sources, whereas the MVDR spectrum is unable to do so. MVDR identifies 41 degrees.

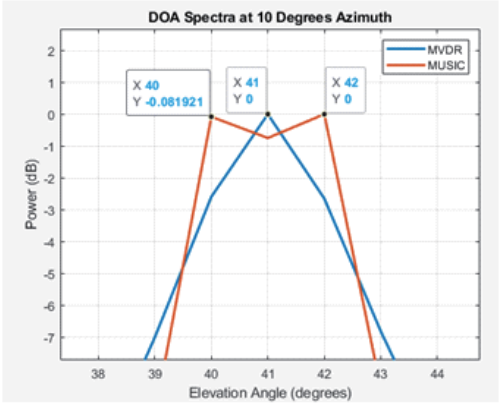

FIGURE 16. DOA spectrum for closely spaced angles 40 and 42 degrees in MVDR and MUSIC.

The designed uniform linear array (ULA) has the ability to scan only between scan angles of −90° and +90°. For a single value of elevation, we can scan for the azimuth angles using ULA. Hence, we design another uniform rectangular array to scan in both azimuth and elevation angles for all 360° scan ranges. Using a 10-by-5 uniform rectangular array (URA), the DOA is estimated. The element spacing between each row and column is kept at 0.3 lambda and 0.5 lambda, respectively. The array geometry is shown in Figure 17(a). The 3D directivity pattern of the array is shown in Figure 17(b).

A URA is capable of estimating both the azimuth and elevation angles. Assuming that the first signal impinges on the URA at 30° in azimuth and 40° in elevation, while the second signal impinges at −10° in azimuth and 15° in elevation, Figure 18 shows the 3D spectrum of the URA for the frequency 5 GHz using beam scan, MVDR, and MUSIC algorithms. The MUSIC algorithm has a better resolution than beam scan and MVDR.

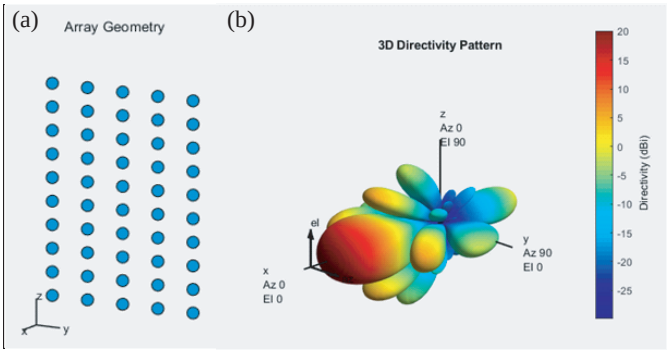

FIGURE 17. (a) URA geometry and (b) 3D directivity pattern of URA.

Adaptive beamforming is the process that produces radiated beams in the direction of desired signals and cancels the beams of interfering signals. There are three types of beamforming techniques that are discussed here. As in the DOA algorithm, where the URA is found to be better than the ULA, these AB algorithms are tested with the designed URA. A phase shift beamformer is used to separate the noise from the signal when the received signal consists of noise. In the presence of a strong interference signal, the phase shift beam former cannot detect the exact signal. So, we use adaptive beam forming to extract the desired signal from the received signal, which consists of signal, noise, and interference. Three beamforming algorithms are illustrated: the phase shift beamformer (Phase Shift), the minimum variance distortion less response (MVDR) beamformer, and the linearly constrained minimum variance (LCMV) beamformer. Figure 19 shows the signal's baseband representation as a simple rectangular pulse. This is the generated signal.

It is assumed that the signal is received by the array at an azimuth angle of 45 degrees and an elevation angle of 0 degrees. Thermal noise is frequently present in the received signal. The overall outcome includes the signal received and the accompanying thermal noise. A beamformer can be viewed as a spatial filter that suppresses the signal from all directions other than the one desired. The outputs of the phase shift beamformer and MVDR beamformer are illustrated in Figures 20 and 21, respectively, for the generated rectangular pulse signal. From these figures, it can be clearly observed that the URA with MVDR beamformer is able to recover the original signal even in the

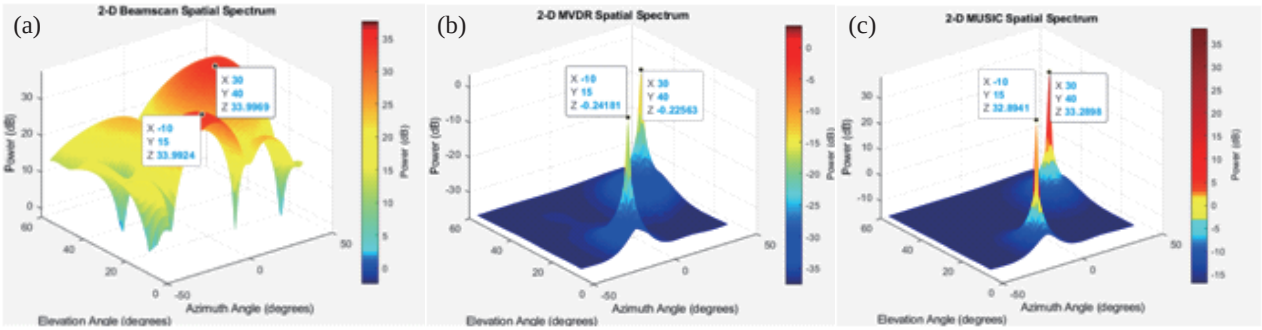

FIGURE 18. DOA estimation at 5 GHZ using (a) Beam scan, (b) MVDR, and (c) MUSIC algorithm.

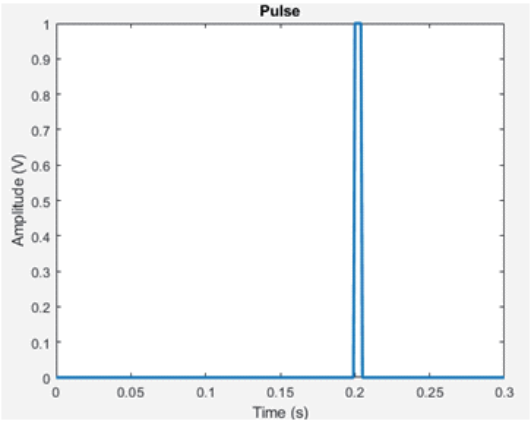

FIGURE 19. Generated Rectangular pulse signal.

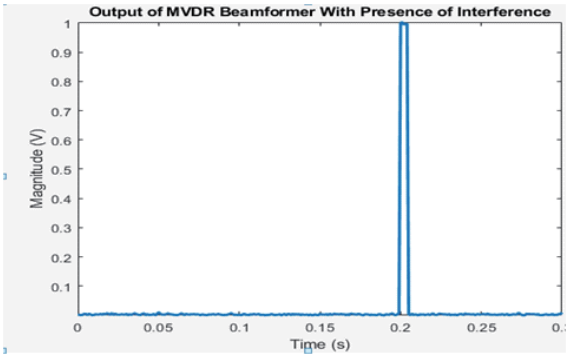

FIGURE 21. Output of MVDR beamformer in the presence of interference signal.

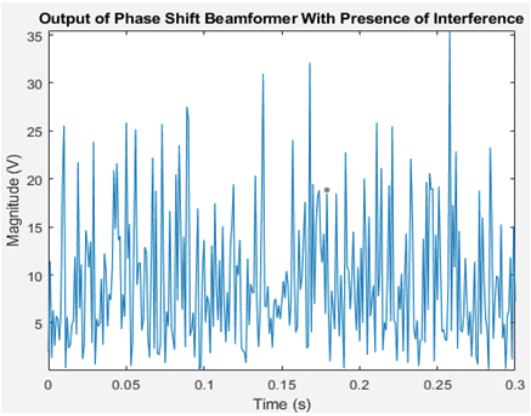

FIGURE 20. Output of phase shift beamformer in the presence of interference.

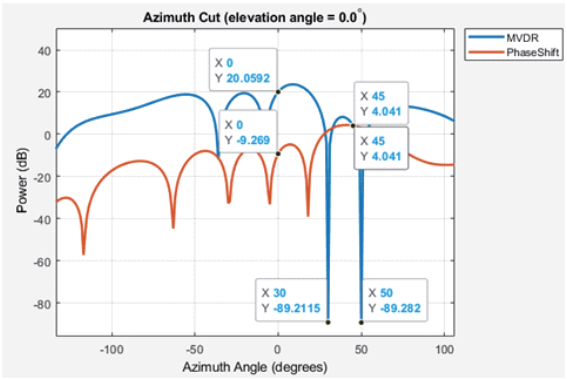

FIGURE 22. Output of MVDR and phase shift beamformer where SOI- 0° and 45° and signal not of interest 30° and 50°.

presence of interference, whereas the phase shift beamformer does not have the capability to recover the original signal.

Figure 22 illustrates that the primary beam of the beamformer is aligned with the intended direction (45 degrees). Subsequently, the beamformer is used to amplify the received signal in the presence of interference. When there is significant interference, the interference signal may mask the target signal. For instance, interference from a neighbouring radio tower can make it impossible for the antenna array to detect signals coming from that direction. Consequently, adaptive beamformers have been developed in order to solve this issue. We have developed a model to represent the arrival of two interference signals originating from azimuth angles of 30 and 50 degrees. The amplitudes of the interference exhibit a significantly greater magnitude than the intended signal. The phase shift beamforming technique is used to extract the signal in the direction of arrival.

When we examine the response pattern of the MVDR beamformer, which is depicted in Figure 22, we notice that there are two significant nulls along the interference directions (30 and 50 degrees). A gain of 0 dB is also maintained by the beamformer along the target direction at 0 and 45 degrees. The MVDR beamformer is able to maintain the target signal while at the same time suppressing the interference signals. Also, as

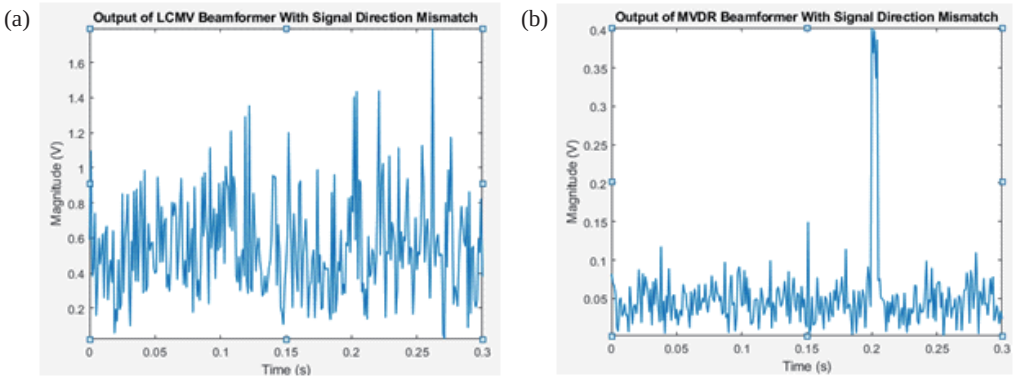

FIGURE 23. (a) output of LCMV beamformer with signal direction mismatch (b) output of MVDR beamformer with signal direction mismatch.

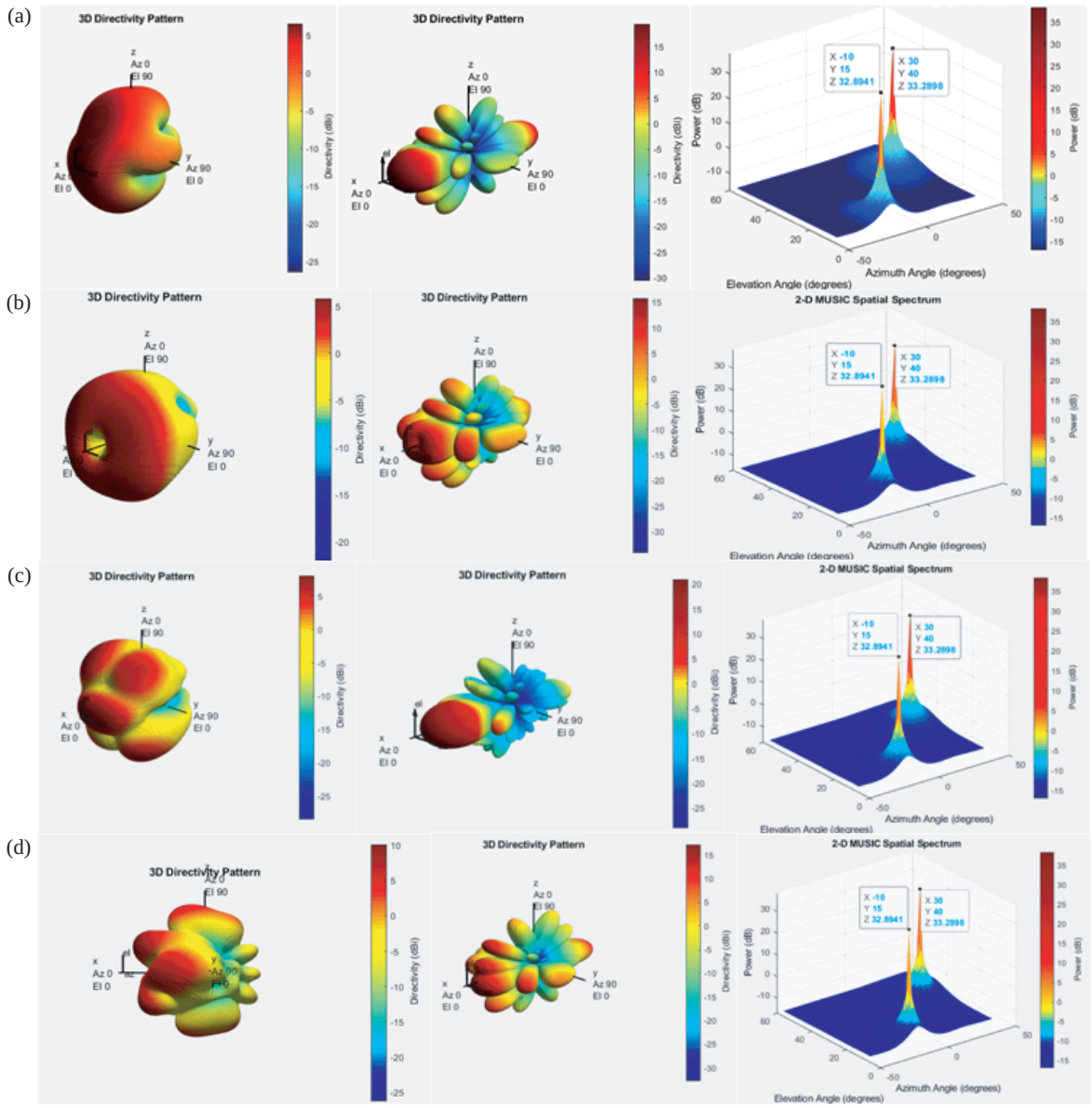

FIGURE 24. 3d pattern of single antenna, URA and Music spectrum for the designed antenna at (a) 10 GHz, (b) 13.2 GHz, (c) 16.2 GHz and (d) 20.5 GHz.

shown in Figure 22, the response pattern from phase shift does not null the interference at all.

Signal direction mismatch refers to a situation in which signals between two devices are not properly aligned or synchro-

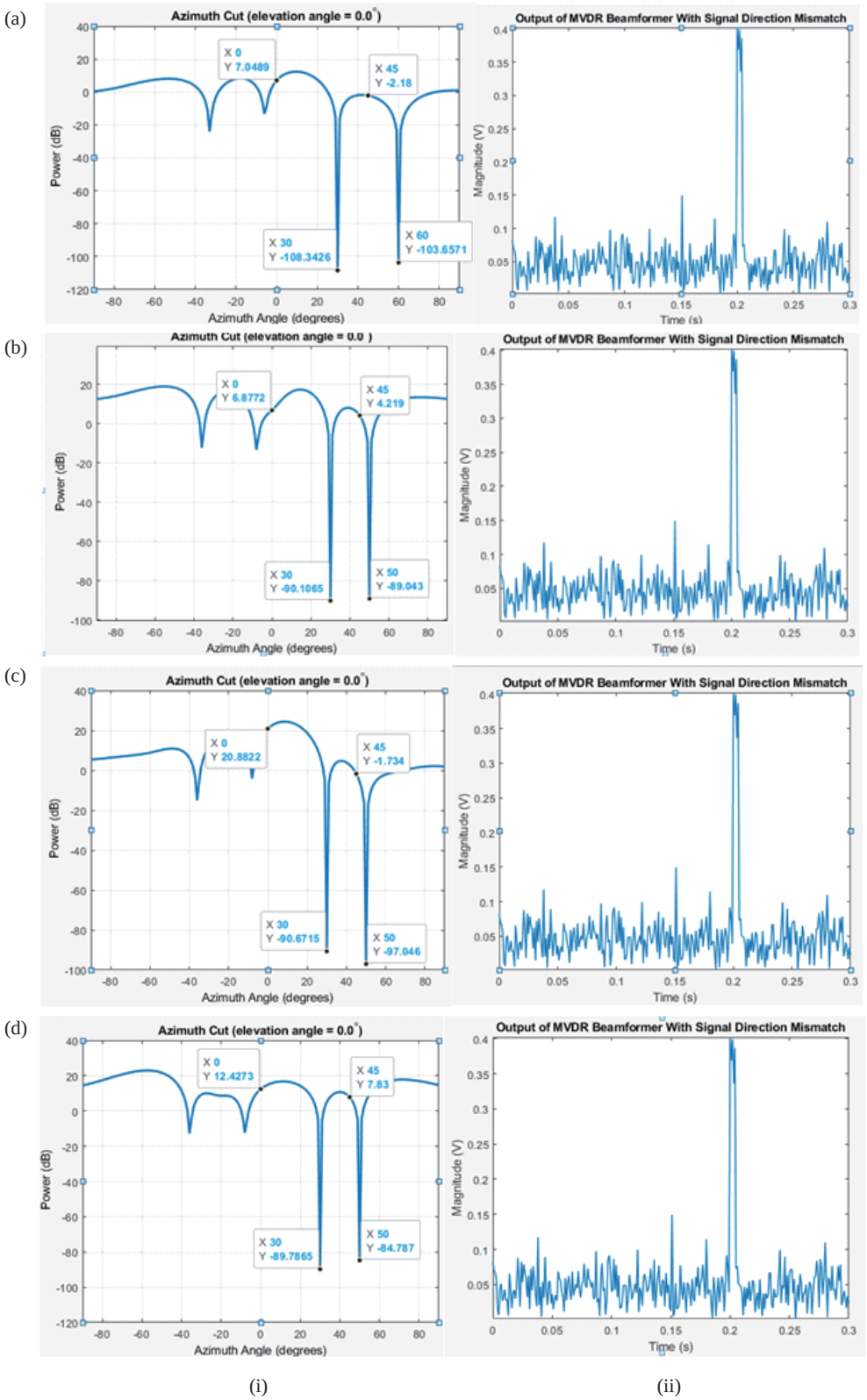

FIGURE 25. (i) Output of MVDR beamformer where SOI-0° and 45° and signal not of interest 30° and 50° and (ii) the output with signal direction mismatch for the frequencies (a) 10 GHz, (b) 13.2 GHz, (c) 16.2 GHz and (d) 20.5 GHz.

nized. This can result in data loss, errors, or incorrect processing of information. For example, if one device is sending signals in a certain direction while another device is expecting signals to come from a different direction, this can lead to a signal direction mismatch, which can happen with satellite systems. Beamforming techniques can be used to resolve signal

direction mismatches in satellite communication systems. In a satellite communication system, a signal direction mismatch can occur when the satellite's antenna is not properly aligned with the ground station or the user's device. This can result in a weaker or distorted signal being received by the ground station or the user, leading to data loss or errors.

Beamforming is a technique used to focus a signal in a particular direction by adjusting the phase and amplitude of multiple antenna elements. By using beamforming, the satellite can adjust its antenna to focus the signal towards the ground station or user device, even if they are located in different directions. This can help to improve the strength and quality of the received signal and reduce the effects of signal direction mismatch. There are several different types of beamforming techniques that can be used in satellite communication systems. Beamforming uses complex signal processing algorithms to adjust the signals after they have been received. Beamforming can be an effective technique for resolving signal direction mismatches in satellite communication systems. Two popular beamforming techniques are the linearly constrained minimum variance (LCMV) beamformer and the minimum variance distortionless response (MVDR) beamformer.

LCMV beamformer is a spatial filter that can attenuate signals from undesired directions while enhancing signals from a desired direction. It operates by minimizing the output power, subject to linear constraints on the filter coefficients. This technique is useful when the direction of the desired signal is known but may not be perfectly aligned with the array of receiving antennas. However, if there is a significant mismatch between the desired signal direction and the actual array response, the LCMV beamformer may not perform well. This is clearly seen from Figure 23(a) which shows the output of LCMV beamformer with signal direction mismatch. On the other hand, the MVDR beamformer is designed to overcome the limitations of the LCMV beamformer in the presence of a signal direction mismatch. The MVDR beamformer uses a more sophisticated mathematical model that considers the spatial covariance matrix of the received signals, and it can adaptively adjust its weights to provide the best possible response to signals coming from different directions. This technique is particularly useful when the desired signal is weak or when there are strong interfering signals from other directions. Therefore, in the case of detecting signal direction mismatch in satellite applications, the MVDR beamformer is often considered to be a better choice, as it can adapt to changes in the signal environment and provide more accurate direction estimates even in the presence of interference or other sources of noise.

The plot in Figure 23(b) shows that the target signal can be detected even though there is a mismatch between the desired and true signal arrival directions. The azimuth range displayed in this analysis is limited to 0–90 degrees in order to facilitate a more precise examination of the response pattern in relation to both signal and interference directions. The MVDR response pattern shows that the beamformer puts the constraints along the specified directions while nulling the interference signals along 30 and 50 degrees. Here we only show the pattern between 0 and 90 degrees in azimuth so that we can see the behaviour of the response pattern at the signal and interference directions better.

Until now, all the popular DOA and AB algorithms have been tested with the proposed antenna array, with our fractal antenna as the element of the array. All these tests are carried out at the first resonating frequency, i.e., 5 GHz. Among all test case scenarios, URA with the MUSIC algorithm and URA with the MVDR algorithm are found to be the best ones for DOA and AB, respectively, for our proposed antenna. Hence, these best cases are now applied to all four resonating frequencies. URA with the MUSIC DOA algorithm is tested for frequencies (a) 10 GHz, (b) 13.2 GHz, (c) 16.2 GHz, and (d) 20.5 GHz, and their responses are plotted in Figure 24.

Similarly, the MVDR AB algorithm with the same URA was found to be the better algorithm for beamforming. Hence, we obtain the output of the MVDR algorithm for beamforming for the other four frequency bands in Figure 25.

By following these steps, we can create a custom antenna and array optimized for satellite applications and use MATLAB to investigate beamforming and direction of arrival algorithms for improved performance. The best DOA and AB algorithms are evaluated for the proposed antenna and array for all its resonating frequencies. After successful recovery of the generated signal, the proposed fractal multiband antenna is concluded to be an ideal candidate for satellite communication.

5. CONCLUSION

In this study, a miniaturised coaxially fed pentaband fractal square antenna is proposed. The antenna resonates at 5 GHz, 10 GHz, 13.2 GHz, 16 GHz, and 20.5 GHz across five bands. Multibands are accomplished with a fractal square antenna. A coaxial pin feed is used to supply the antenna. The fractal square is derived from an initial patch of squares. The fractal characteristic aids in the antenna's miniaturisation. The given antenna has a gain between 4.9 and 9.7 dB and an efficiency between 70% and 98%. Simulation of the proposed antenna was done using the CST microwave studio. The antenna is fabricated, and the measured results are used to create a custom antenna and its array in MATLAB. Beam forming and the direction of arrival algorithm are investigated in MATLAB to find the direction of arrival and beamforming for application in satellite. The antenna's performance is measured in terms of its radiation pattern, impedance matching, and gain. MATLAB provides a powerful tool set for antenna design, array modelling, and beamforming algorithm implementation. By following these steps, we can create a custom antenna and array optimized for satellite applications and use MATLAB to investigate beamforming and direction of arrival algorithms for improved performance. The best DOA and AB algorithms are evaluated for the proposed antenna array for all its resonating frequencies. After successful recovery of the generated signal, the proposed fractal multiband antenna is concluded to be an ideal candidate for satellite communication.

REFERENCES

[1] Chun, D., "Overcoming C-band satellite interference," *Microwave Product Digest*, Oct. 2017.

[2] "Consultation paper on assignment of spectrum for space-based communication services," Telecom Regulatory Authority of India, Apr. 2023.

[3] Maval, G. and M. Bousquet, *Satellite Communications Systems*, John Wiley & Sons, 2020.

[4] Rajmohan, I. J. and M. I. Hussein, "A compact multiband planar antenna using modified L-shape resonator slots," *Heliyon*, Vol. 6, No. 10, e05288, ISSN 2405-8440, 2020.

[5] Prasad, B. S. H. and M. V. Prasad, "Design and analysis of compact periodic slot multiband antenna with defected ground structure for wireless applications," *Progress In Electromagnetics Research M*, Vol. 93, 77–87, 2020.

[6] Yan, N., K. Ma, H. Zhang, and P. Jia, "An SISL triple-band multimode stacked-patch antenna with L-strips for multi-band applications," *IEEE Transactions on Antennas and Propagation*, Vol. 67, No. 2, 1284–1288, Feb. 2019, doi: 10.1109/TAP.2018.2883565.

[7] David, R. M., M. S. Aw, T. Ali, and P. Kumar, "A multiband antenna stacked with novel metamaterial SCSRR and CSSRR for WiMAX/WLAN applications," *Micromachines (Basel)*, Vol. 12, No. 2, 113, 2021.

[8] Soliman, A., D. Elsheakh, E. Abdallah, and H. El-Hennawy, "Multiband printed metamaterial inverted-F antenna (IFA) for USB applications," *IEEE Antennas and Wireless Propagation Letters*, Vol. 14, 297–300, 2015.

[9] Nallapaneni, S. and P. Muthusamy, "Design of multiband fractal antenna loaded with parasitic elements for gain enhancement," *Int. J. RF Microw. Comput. Aided Eng.*, Vol. 31, No. 6, Jun. 2021.

[10] Subbu, R. and R. Rani, "CPW-fed octagonal-shaped metamaterial-inspired multiband antenna on frequency selective surface for gain enhancement," *Applied Physics A*, Vol. 128, No. 7, 594, 2022.

[11] Khan, O. M., Z. Ul Islam, I. Rashid, F. A. Bhatti, and Q. Ul Islam, "Novel miniaturized koch pentagonal fractal antenna for multiband wireless applications," *Progress In Electromagnetics Research*, Vol. 141, 693–710, 2013.

[12] Li, D. and J. Mao, "A Koch-like sided fractal bow-tie dipole antenna," *IEEE Transactions on Antennas and Propagation*, Vol. 60, No. 5, 2242–2251, May 2012.

[13] Gupta, M., V. Mathur, A. Kumar, V. Saxena, and D. Bhatnagar, "Microstrip hexagonal fractal antenna for military applications," *Frequenz*, Vol. 73, Nos. 9–10, 321–330, 2019.

[14] Samsuzzaman, M. and M. T. Islam, "Inverted S-shaped compact antenna for X-band applications," *The Scientific World Journal*, 604375, 2014.

[15] Vijayvergiya, P. L. and R. K. Panigrahi, "Single-layer single-patch dual band antenna for satellite applications," *IET Microwaves, Antennas and Propagation*, Vol. 11, No. 5, 664–669, 2017.

[16] Yang, X., L. Ge, Y. Ji, X. Zeng, and K. M. Luk, "Design of low-profile multi-band half-mode substrate-integrated waveguide antennas," *IEEE Transactions on Antennas and Propagation*, Vol. 67, No. 10, 6639–6644, Oct. 2019.

[17] Surendrakumar, P. and B. Chandra Mohan, "A triple-frequency, vertex-fed antenna for WLAN/WiMAX applications [Antenna Applications Corner]," *IEEE Antennas and Propagation Magazine*, Vol. 60, No. 3, 101–106, 2018.

[18] Kumar, R., G. S. Saini, and D. Singh, "Compact tri-band patch antenna for Ku band applications," *Progress In Electromagnetics Research C*, Vol. 103, 45–58, 2020.

[19] Chinnagurusamy, B., M. Perumalsamy, and A. S. T. Sarasam, "Design and fabrication of compact triangular multiband microstrip patch antenna for C- and X-band applications," *International Journal of Communication Systems*, Vol. 34, No. 15, e4939, 2021.

[20] Agrawal, P. and M. Shandilya, "MATLAB simulation of subspace based high resolution direction of arrival estimation algorithm," *International Journal of Computer Applications (0975–8887)*, Vol. 130, No. 15, 22–27, Nov. 2015.

[21] Jose, A., "Simulation of an adaptive digital beam former using matlab," *International Journal of Advanced Research in Basic Engineering Sciences and Technology (IJARBEST)*, Vol. 2, No. 12, 10–18, Dec. 2016.

[22] Varnikha, N. and P. Jothilakshmi, "Modified minkowski multiband fractal antenna for satellite applications," *International Journal of Microwave & Optical Technology*, Vol. 18, No. 4, 367–376, Jul. 2023.

[23] Jothilakshmi, K. and P. Jothilakshmi, "Design of multilayer microstrip patch antenna for satellite application," *International Journal of Innovative Research in Computer and Communication Engineering*, Vol. 5, Special Issue 3, 190–195, Apr. 21, 2017.

[24] Jothilakshmi Vishnu Prakash, P. and R. Srinivasan, "Miniaturised multiband two-element coaxial continuous transverse stub antenna for satellite C-band application," *IET Microwaves, Antennas and Propagation*, Vol. 8, No. 7, 474–481, May 2014.

[25] Vijetha, T. and D. R. Krishna, "A frequency reconfigurable MIMO antenna with UWB sensing for multi-band operations," *International Journal of Microwave & Optical Technology*, Vol. 18, No. 1, 57–68, Jan. 2023.

[26] Kashyap, N., D. Singh, and Geetanjali, "A compact multiband annular-slotted patch rectenna for efficient energy harvesting," *International Journal of Microwave & Optical Technology*, Vol. 18, No. 3, 284–291, May 2023.

[27] Patel, D. H. and G. D. Makwana, "Multiband antenna for GPS, IRNSS, Sub-6 GHz 5G and WLAN applications," *Progress In Electromagnetics Research M*, Vol. 116, 53–63, 2023.